Spin-wave measurements on MBE-grown zinc-blende structure MnTe by inelastic neutron scattering

B. Hennion*
Laboratoire Léon Brillouin, CEA-CNRS, CE Saclay, 91191 Gif-sur-Yvette cedex, France

W. Szuszkiewicz,† E. Dynowska, E. Janik, and T. Wojtowicz‡
Institute of Physics, Polish Academy of Sciences, Al. Lotników 32/46, 02-668 Warsaw, Poland

(Received 28 June 2002; revised manuscript received 11 September 2002; published 31 December 2002)

Spin-wave excitations of a MBE-grown single crystal of MnTe with a zinc-blende structure have been measured by inelastic neutron scattering in the type-III antiferromagnetic low-temperature phase of this compound. The experimental data have been modeled with a Heisenberg Hamiltonian including isotropic exchanges and magnetic anisotropy. Exchange constants and anisotropy terms have been estimated, which allowed a discussion on the relative importance of distant neighbors. The relevance of anisotropic exchanges is also discussed. The assumption of a collinear spin arrangement provides a consistent description of the spin-wave spectrum, including inelastic-neutron-scattering cross section. The temperature dependence of the spin waves revealed an anomalously strong damping, which starts well below the transition temperature.

DOI: 10.1103/PhysRevB.66.224426 PACS number(s): 75.25.+z, 61.12.−q, 75.30.Ds, 75.50.Pp

I. INTRODUCTION

The knowledge of magnetic exchange interactions between magnetic ions is a key factor for the understanding of the properties of diluted magnetic (semimagnetic) semiconductors (DMS's). The best known group of such materials is based on II-VI tellurides containing Mn and possess the zinc-blende (ZB) structure, such as $Zn_{1-x}Mn_xTe$, $Cd_{1-x}Mn_xTe$, $Hg_{1-x}Mn_xTe$, or $Mg_{1-x}Mn_xTe$. It is widely accepted that the predominant mechanism of magnetic interactions between Mn^{2+} ions in this group of DMS's is the superexchange (see, e.g., Anderson[1,2]) mediated by the Te anions.[3–7] Because of the ZB structure the antiferromagnetic (AF) character of these interactions causes frustration which, added to disorder, induces at low temperatures a spin-glass-like state in the low Mn concentration range of the phase diagram. In particular, for the mixed crystals containing Zn or Cd such a state has been observed in the composition range $0<x\lesssim 0.6$.[8–12] With the increase of Mn concentration x above 0.6 one expects first a short-range order (creation of magnetic clusters), followed by a long-range order, and finally a true AF order. Bulk samples with a very high Mn concentration cannot be grown in the ZB structure by equilibrium techniques since they undergo a structural transition towards a hexagonal NiAs structure, which is the natural structure of pure bulk MnTe.[13] A single ZB crystallographic phase of bulk crystals could have only been obtained in the case of $Cd_{1-x}Mn_xTe$ for $x\lesssim 0.77$ and in the case of $Zn_{1-x}Mn_xTe$ for $x\lesssim 0.86$.[14]

ZB DMS's with any Mn composition can be grown with the use of nonequilibrium techniques such as molecular-beam epitaxy (MBE), because the ZB structure for very high x is stabilized by the inherent axial strain, imposed by the substrate. The growth of pure ZB MnTe was first demonstrated by Durbin *et al.*[15] This opened the path for the studies of very thick, bulklike, epitaxial layers of ZB MnTe—the magnetic component of all Mn-based DMS tellurides—and for further progress in the understanding of this potentially important, in view of spintronic applications, group of materials. In particular, the studies of MBE-grown weakly diluted magnetic semiconducor layers allowed the magnetic phase diagrams to be completed.[16–23] It was also shown that pure ZB MnTe undergoes a first-order transition at the Néel temperature $T_N\approx 65$ K and that below T_N it orders magnetically in a type-III AF structure.[16,17,19] This confirmed the suggestions deduced from the first elastic-neutron scattering measurements performed on $Cd_{1-x}Mn_xTe$ (Refs. 24 and 25) and $Zn_{1-x}Mn_xTe$ (Refs. 26 and 27) bulk crystals. The type-III AF magnetic order, which will be presented in detail in Sec. II B, is expected when strongly dominant nearest-neighbor and next-nearest-neighbor interactions (described by the exchange integrals usually named J_1 and J_2, respectively) are both antiferromagnetic, and has been predicted by a theoretical analysis[28,29] devoted to possible AF orders of magnetic crystals with a face-centered-cubic (fcc) structure.

The relative importance of isotropic exchange interactions for different shells of neighbors is a fundamental factor for the magnetic structure of DMS's. All Mn-Mn superexchange interactions are mediated by bridging via Te ions and the nature of the bridging may strongly affect the hierarchy of the exchanges, usually thought of in terms of Mn-Mn distances. Many theoretical papers have addressed this issue. The fast decrease, limiting the relevant interactions to first and second neighbors,[3,7] was found overestimated and many models[30–35] suggest a significant contribution of more distant third and fourth neighbors. Detailed theoretical calculations of the superexchange interaction using realistic linear combination of atomic orbitals (LCAO) energy-band calculations,[36] *ab initio* calculations,[37] or the three-level model of the band structure[38] have been performed, and pointed out a spatial dependence of the exchange interactions more complex than a simple power form, with even the possibility[36,37] that J_4 could be larger than J_2.

Magnetization measurements at high magnetic fields and very low temperatures for highly diluted magnetic semicon-

ductors $Zn_{1-x}Mn_xX$ (X=S, Se, Te) (Refs. 39 and 40) and $Cd_{1-x}Mn_x$Te (Ref. 41) have been interpreted in this way, assuming a random distribution of Mn. However, the adequacy of this interpretation for large Mn concentration or for pure ZB MnTe is not obvious. Indeed, LCAO theoretical calculations[42] point out a significant dependence of the exchange constants on the Mn concentration in $Cd_{1-x}Mn_x$Te, strongly affecting the exchange between more distant neighbors, and mainly related to the evolution of the contribution to the exchange of the electron-hole interaction.

Another important point is the possible occurrence of anisotropic contributions to the total exchange interaction, allowed in the ZB structure because of the lack of center of symmetry. Hybridization of Mn d states with sp band states of Te, arising because of the anion spin-orbit interactions, may induce anisotropy in the superexchange spin-spin coupling of Mn nearest neighbors. Such a possibility of Dzialoshinski-Moriya (DM) anisotropic exchange[43,44] in the ZB structure has been invoked by many authors.[7,35,36,45–51]

Finally, the anisotropy of the nearest-neighbor exchange interaction due to the tetragonal distortion of the nuclear unit cell in the magnetically ordered AF III phase has also been analyzed, either through the determination of exchange striction[35] or through the angular dependence of the nearest-neighbor exchange.[4,52–54]

All numerical data cited in the literature and related to exchange integrals and magnetic anisotropies are based on experiments performed either on Mn-containing mixed crystals or on highly diluted magnetic semiconductors. This implies large variations of many parameters: disorder and frustration in the high Mn concentration range, and the importance of the local symmetry and environment for diluted systems, which has made it difficult to get definite conclusions on the pure sytem by mere extrapolation. The access to these quantities with the use of pure ZB MnTe remained therefore an appealing goal and put forward the possibility to determine them via the measurements of the spin-wave excitations of the AF ordered phase.

The first experimental results of this kind have been obtained by neutron scattering on $Cd_{0.35}Mn_{0.65}$Te mixed crystals (Refs. 25 and 55) and more detailed inelastic-neutron-scattering studies have been reported for $Cd_{0.33}Mn_{0.67}$Te (Refs. 56 and 57) and for $Zn_{0.35}Mn_{0.65}$Te.[56] Analysis of these data was done with a quasiharmonic spin-wave approximation including nearest-neighbor exchange and next-nearest-neighbor exchange (J_1 and J_2, respectively): both were found antiferromagnetic as predicted for superexchange mediated by Te anions. However, no inelastic-neutron-scattering data have been obtained so far for crystals with perfect long-range type-III AF magnetic order, because of the small sample volume (mm^3 size).

The zone-center magnon mode[58,59] as well as its temperature dependence[61,62] has been observed by one-magnon Raman scattering for MBE-grown MnTe in the AF III structure. A frequency of 33.6 cm^{-1} was found, with only a small variation with a substitution of Mn by Cd, Zn, or Mg.[60,59] But this value corresponds to a combination of magnetic anisotropy and exchange and only the use of the experimental value of T_N allows to obtain a model-dependent estimation of the parameters.

The improvement of the neutron-scattering technique, especially related to the use of focusing devices on three-axis spectrometers (TAS) has strongly extended the possibility of inelastic-scattering measurements, and samples of mm^3 size may now be investigated in favorable cases. The case of MnTe is indeed a favorable one since several micron thick MBE-grown samples are now available[63–65] and the magnetic moment of Mn^{2+} has a high value of almost $5\mu_B$.[4,66] Recent developments of the experimental technique at the Orphée reactor of the Laboratoire Léon Brillouin (LLB) at Saclay, France, with a beam tube redesigned to optimize the thermal beam flux available on the 2T TAS, offered the possibility to measure the spin-wave spectrum of AF III MnTe. The results of these experiments are presented in this paper.

The paper is organized as follows. In Sec. II details concerning the sample growth and its structural characteristics are reported. The spin-wave measurements at low temperature, including details related to the magnetic domain compositions of the sample, are presented in Sec. III. The temperature dependence of a few modes, related to the magnetic transition of the system, is reported in Sec. IV. The analysis of the results and a subsequent discussion can be found in Sec. V.

II. SAMPLE GROWTH AND CHARACTERISTICS

A. Growth and crystalline properties

A 6-μm-thick ZB MnTe layer has been grown by MBE in the EPI 620 system at the Institute of Physics of the Polish Academy of Sciences in Warsaw. The growth was performed on an epi-ready semi-insulating GaAs substrate with (001) orientation (2° misoriented towards the [011] direction), with a very thin ZnTe buffer followed by a thicker (2 μm) CdTe buffer layer. The growth of the MnTe layer was realized in Te-rich conditions from elemental Mn and Te sources (more detailed information about the growth can be found elsewhere.[63–65])

X-ray diffraction was used to check the lack of other phases and to verify the crystal quality of the sample. Single-phase growth of the MnTe layer has been confirmed using a low-resolution diffractometer. A high-resolution x-ray diffractometer in double-crystal geometry was used to assess the sample quality. The full width at half maximum (FWHM) values for (004) rocking curves measured for the CdTe buffer and MnTe layer were determined as $4'$ and $14'$, respectively. Reciprocal space mapping of (004) and $(\overline{335})$ Bragg reflections performed to better understand the sample characteristics are illustrated in Fig. 1. The mapping of the (004) symmetrical reflection confirms that the main origin of the rocking curve broadening is the sample mosaicity [Fig. 1(a)] and that of the $(\overline{335})$ asymmetrical reflection [Fig. 1(b)] allows to estimate the strain state of the layer, by determining the in-plane (a_{xy}) and out-of-plane (a_z) lattice-parameter values. A slight tetragonal distortion has been found for both the MnTe layer (a_{xy}=6.3366 Å, a_z=6.3411 Å) and the CdTe buffer (a_{xy}=6.4790 Å, a_z=6.4848 Å). Both layers

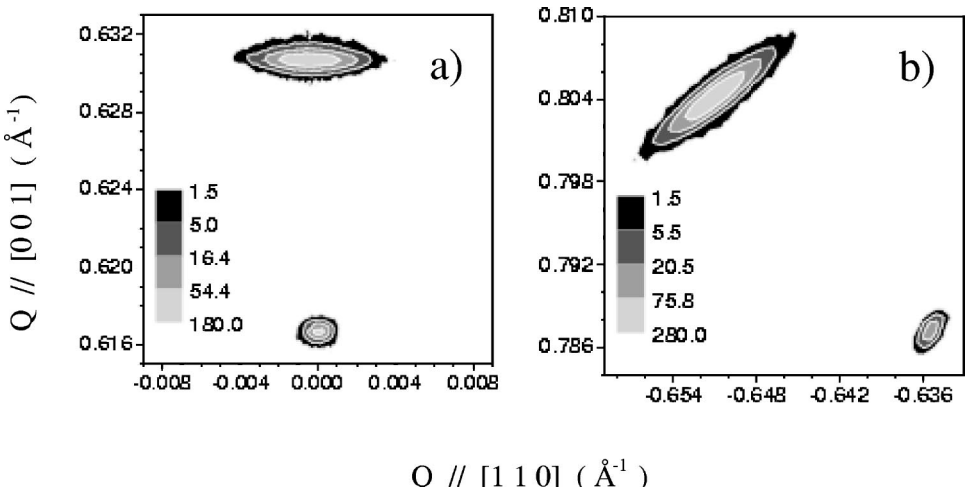

FIG. 1. Reciprocal space maps taken for the MnTe/CdTe/GaAs(001) sample: (a) (004), (b) $(\bar{3}3\bar{5})$ reflections. The MnTe layer and the CdTe buffer are shown in the upper and the lower part of this figure, respectively; the area corresponding to the GaAs substrate is not presented.

were residually compressively strained because of the difference between thermal-expansion coefficients of the GaAs substrate and deposited layers during the cooling process after the MBE growth.

The temperature dependence of the lattice parameter has been determined by elastic neutron diffraction. A monochromatic neutron beam, coming from a cold source, was obtained with a double monochromator, made of pyrolytic graphite in (002) reflection [PG(002)], and filtered by cold beryllium to reduce higher-order contamination. The diffracted beam was analyzed by a PG(002) crystal, with 20′ collimation on each side. This yielded a Q resolution of 4×10^{-3} Å^{-1} (FWHM) for neutrons of wave vector $k_i=1.18$ Å^{-1}, which have been used for the study of the crystal structure. The sample with a surface of ≈3 cm^2 was mounted in an aluminum can containing helium exchange gas, and fixed on the cold finger of a closed cycle refrigerator.

The temperature dependence of the lattice parameters reported in Fig. 2 has been obtained by analyzing the splitting observed when measuring the (002) Bragg reflection at low temperatures. Due to the negative Fermi length of Mn, the intensity of the (002) reflection observed by neutron diffraction was high, even in the ZB structure, and the contamination by the equivalent reflection of the CdTe buffer was negligible.

The result shown in Fig. 2 illustrates the tetragonal structural distortion $(\Delta a/a=0.3\%)$ which the sample undergoes below the magnetic phase transition at low temperature. The transition was found to be very abrupt and consistent with a first-order character, but with only a small step, which was better evidenced on the temperature dependence of the Bragg magnetic signal.

Contrary to previous measurements performed on ZB MnTe (Refs. 16 and 19 and $Zn_{0.06}Mn_{0.94}Te$,[35] we did not find a significant difference between the Néel temperature and the temperature of the structural distortion (in our case the difference was smaller than 5 K, which is within the accuracy of the splitting determination). This is likely related to the large thickness of our sample and to a very small residual strain (almost fully relaxed state), as already evidenced by the x-ray-diffraction data taken at room temperature.

The observation of a splitting is a direct consequence of the sample partition into different domains in the tetragonal phase. Indeed the structural distortion consists of an elongation of one axis of the high-temperature structure. The preferred axis at the transition is related to the strain induced at the interface by the buffer layer. In our case (CdTe buffer layer) this favors the in-plane axes and, because of the symmetry of the system, gives rise to two equivalent domains. Furthermore, the sample thickness is such that the third domain with the elongation perpendicular to the layer plane is also populated.

As the effects deriving from this domain partition will be important in the data analysis of inelastic-neutron-scaterring measurements, we will use the following rules to label the axes, as illustrated in Fig. 3. The X,Y,Z axes define the real space of the sample, with Z being perpendicular to the layer, and XZ defining the neutron-scattering plane. x,y,z axes are attached to a given domain, with the assumption that z is always along the long axis of the tetragonal cell, and ξ,η,ζ span the associated reciprocal space. We then will speak of domains X, Y, or Z when the z axis is along the X, Y, or Z axis, respectively. We will neglect the small lattice distortion $(\approx7\times10^{-4})$ due to the residual compressive strain at room temperature, and consider a unique set of lattice parameters ($a=a'$ and $c=c'$ in Fig. 3). The domain populations have been deduced from the intensity ratio of the split (002) peaks, yielding 22% of the Z domain and 39% of domains X or Y.

B. AF III magnetic structure

Below $T_N\approx65$ K magnetic Bragg peaks appear, in agreement with the AF III magnetic structure already evidenced for ZB MnTe by Giebultowicz *et al.*[19] The temperature dependence of the $(10\frac{1}{2})$ reflection, characteristic of such a structure as explained below, is presented in Fig. 2, and the first-order character of the transition is seen at T_N by the sudden drop of the magnetic intensity, without the tail due to critical scattering normally associated with a second-order phase transition. No hysteresis has been detected, within our

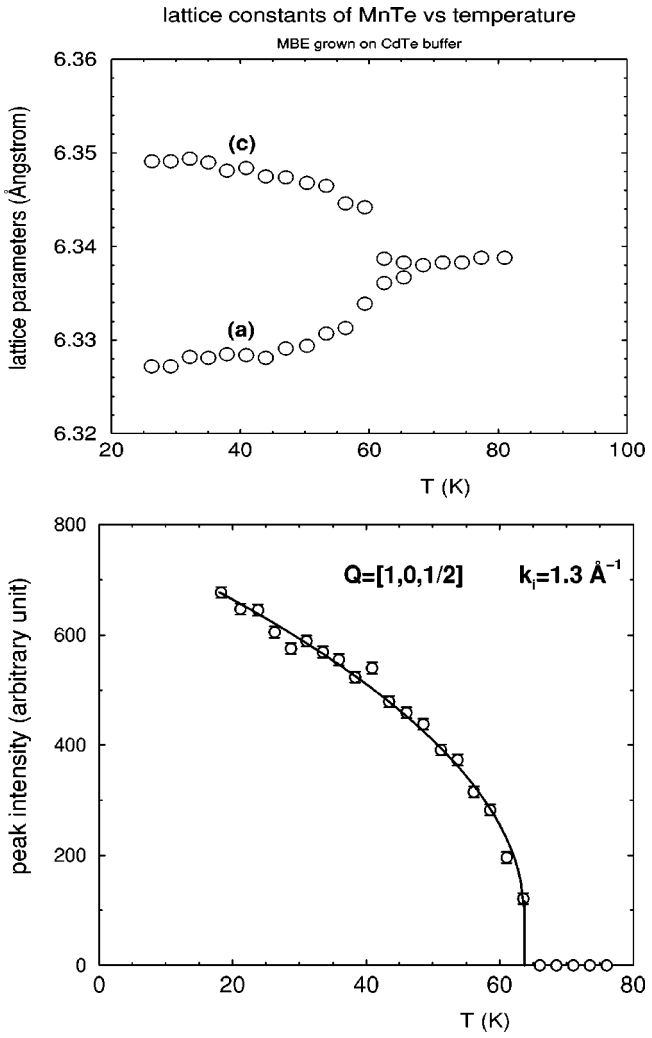

FIG. 2. Top: temperature dependence of the lattice parameter of MnTe illustrating the tetragonal distortion as deduced from the splitting of the (002) Bragg reflection. Bottom: temperature dependence of the $(10\frac{1}{2})$ antiferromagnetic reflection.

experimental accuracy of ≈ 1 K, accounting for the temperature increment of the measurements done in cooling or heating the sample.

The AF III magnetic structure, illustrated in Fig. 4, is made of two sublattices of perfect AF ordered planes (xy planes of the figure), stacked along z, the long axis of the tetragonal structure. A sublattice consists in a stacking along z of AF planes with an interplane distance of c, with a spin reversal every c (e.g., planes containing spins 1 and 3 in Fig. 4).

As it has been determined first for ZB β-MnS (Ref. 67) and then for ZB MnTe,[19] the spin direction is within the xy plane, but its exact direction in the plane could not be specified. The sublattices are deduced from each other by a translation of the form $[\frac{1}{2}0\frac{1}{2}]$ if regarding their spin positions (e.g., from spin 3 to spin 2 in Fig. 4), but the relative orientation of the spins is not uniquely defined. Indeed it can be shown that the interactions between a given spin of a sublattice and its nearest neighbors of the other sublattice have a

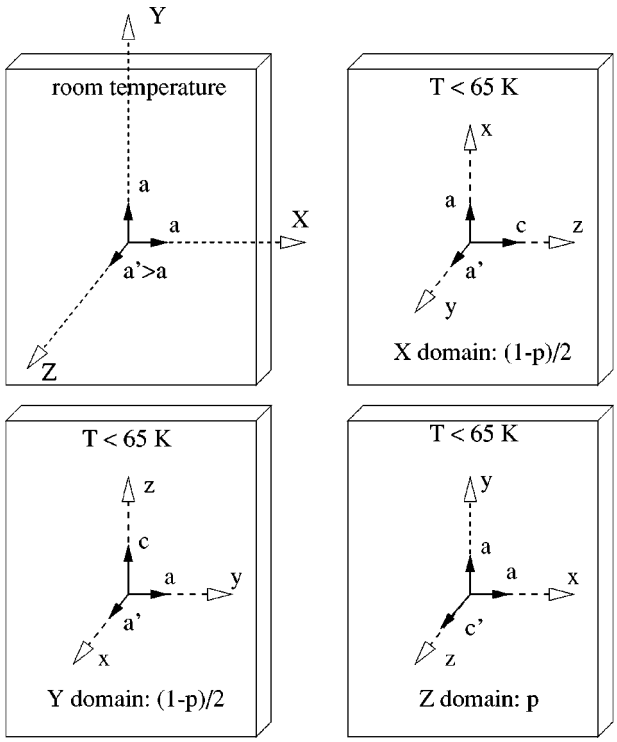

FIG. 3. Schematic view of the crystal structure of ZB MnTe grown on a CdTe buffer layer: starting from a slightly tetragonally distorted structure at room temperature ($a<a'$), three types of domains are found in the low-temperature phase. c or c' is the long axis resulting from the transition. p is the percentage of Z domain.

null resultant, even when taking the tetragonal lattice distortion into account.

The respective alignment of the two sublattices is then defined by other forces. The collinear structure is not the only solution and an ordering with a spin rotation between sublattices is possible. Keffer,[45] analyzing the ground state of ZB β-MnS, suggested a 90° rotation, hereinafter referred to as the Keffer structure, but a canted structure with an arbitrary angle cannot be excluded.[68] This kind of canting is made possible by the noncentrosymmetric character of the

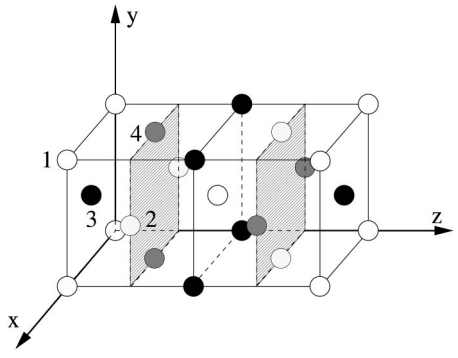

FIG. 4. Magnetic structure of AF III MnTe. Only positions of magnetic Mn atoms are shown. Spins 1 and 3 are antiparallel, as are spins 2 and 4. When the structure is collinear, spins 1 and 2 are parallel, while in the noncollinear structure proposed by Keffer[45] spins 1 and 2 are perpendicular.

nuclear structure which allows anisotropic exchanges such as the DM exchange.

The collinear state has been shown favored in the pure system,[69] but is very sensitive to disorder. Monte Carlo simulations[70] revealed a complex phase diagram for a ZB diluted magnetic semiconductor, where above 85% of Mn the magnetic system exhibits a reentrant behavior going from a paramagnetic to a long-range collinear AF III phase and finally to a long-range noncollinear AF III phase when lowering the temperature. Because of domain effects, magnetic neutron-diffraction measurements can only demonstrate that the spins lie within the AF planes. In the following, we will use the assumption of a collinear magnetic structure to analyze our experimental data. We will discuss in Sec. V the consistency of this assumption.

As may be seen in Fig. 4, the magnetic lattice has in fact a body-centered tetragonal structure, with a doubling of the nuclear cell along z and with four spins in the magnetic unit cell. Keeping the indexing of the nuclear lattice, this induces the selection rule $h+k+2l=2n+1$, and yields that only Bragg peaks with $h+k$ odd and $l=(2m+1)/2$ have a nonzero magnetic structure factor. Magnetic domains are in the same ratio as the nuclear ones and within each of these domains subdomains, depending on the multiplicity of the easy-magnetization axis in the plane, could also exist. This last effect has no consequence for the spin-wave determination, contrary to the first type of domains. The domain populations determined from the intensity ratio of the $(10\frac{1}{2})$ and $(\frac{1}{2}01)$ were consistent with those deduced from the nuclear peaks' intensities.

III. SPIN-WAVE MEASUREMENTS

Inelastic-neutron-scattering measurements have been performed on a thermal beam, with a configuration optimized for maximum intensity. The incident beam was delivered by a PG(002) monochromator, vertically bent to focus the beam on the sample, and the scattered beam was analyzed with a PG(002) crystal horizontally and vertically bent to focus on the detector. Measurements have been performed at constant final wave vectors of $k_f=2.662$ Å^{-1} and $k_f=3.85$ Å^{-1}, with a graphite filter positioned between the sample and the analyzer to reduce higher harmonics. No Soller slit collimators were used, which resulted in an energy resolution[71] of $\delta E\approx 0.2$ THz in the elastic position at $k_f=2.662$ Å^{-1} and a Q resolution of $\delta Q\approx 0.04$ Å^{-1} (both values corresponding to FWHM).

The weakness of the scattered intensity enhanced the difficulties commonly encountered in this kind of measurements: parasitic signals, nonconstant background at low scattering angles, etc. Therefore we had to check carefully the consistency of the results. For instance, we realized that our signal was sensitive to the inelastic scattering from the helium exchange gas filling the sample can, which evolved significantly with temperature in the range of interest for this study. This gave rise to spurious effects and made the determination of the temperature dependence of the magnetic signal more difficult.

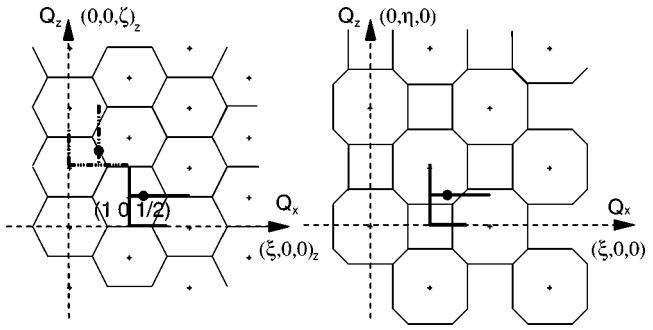

FIG. 5. Scattering planes for the domains Z (left) and Y (right). The projections of the trajectories in the Q_XQ_Z plane along which measurements have been performed are indicated by broad lines. Domain X is deduced from domain Z by the correspondence $(\xi,0,0)_Z\Rightarrow(0,0,\zeta)_X$ and $(0,0,\zeta)_Z\Rightarrow(0,\eta,0)_X$. The corresponding trajectory is indicated by the dot-dashed lines.

However, the main experimental difficulty came from the polydomain character of the sample. It decreases the effective scattering volume to less than 1 mm^3 per domain, the total MnTe volume being about 1.8 mm^3 (6 μm thickness and a surface of about 3 cm^2). Moreover, the contributions of different domains could be superimposed in a given measurement, leading to ambiguity in the assignment of the observed modes.

The definition of the Q position in a measurement will be given in the conjugate space of X,Y,Z and written as Q_X,Q_Y,Q_Z. An inelastic-neutron-scattering measurement at a given Q value yields the superposition of three (ξ,η,ζ) contributions, weighted by the population of the domains. When the scattering plane is defined as the Q_XQ_Z plane, the scattering planes deduced for the three domains are shown in Fig. 5, with the trajectories along which the measurements have been performed.

The temperature dependence provided an important check of the magnetic character of the observed signal. This is illustrated in Fig. 6, where a comparison of measurements performed at $T=13$ K and $T=75$ K shows the disappearance of the spin-wave signal above the Néel temperature. To overcome the difficulty arising from domain effects we proceeded in the following way: we performed some measurements at equivalent Q positions corresponding to different ratios of the domain contributions and we compared the results to a realistic spin-wave model, including a calculation of the inelastic-neutron-scattering cross section, which was refined self-consistently. Then, as far as possible, we used a continuity argument to complete step by step the spin-wave spectrum. An example of such a procedure is illustrated in Fig. 7, which shows results of measurements performed at Q values corresponding to the zone center of domain X,$Q=(\frac{1}{2},0,1)$ (population of 39%), and to that of domain Z,$Q=(1,0,\frac{1}{2})$ (22%). Each measurement contains three contributions: that of a zone-center spin wave, and those of the two other domains, which at this special position have the same frequency. This explains the double-peak feature observed in the measurements with open circles in the top and bottom panels of Fig. 7. In each panel of the same figure a measure-

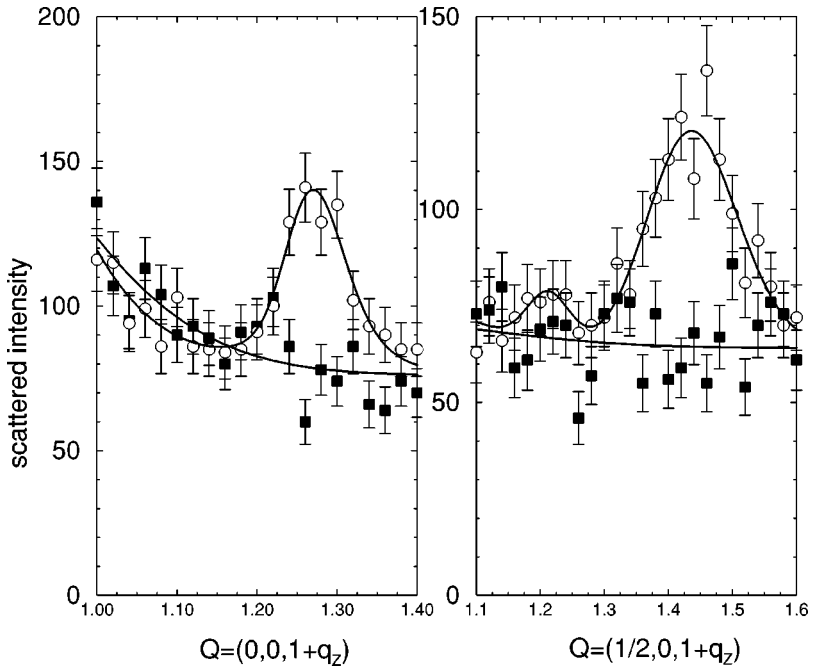

FIG. 6. Verification of the magnetic character of the scattering in constant-ν scans, with $k_f = 3.85$ Å^{-1}. Open symbols correspond to measurements at $T=13$ K, full symbols at $T=75$ K. Left: $\nu=2.8$ THz, $Q=(0,0,1+q_Z)$. The peak corresponds to superimposed equivalent contributions of $(1+\xi,0,0)$ of domain Y and $(0,1+\eta,0)$ of domain X and defines the magnon mode marked 1 in Fig. 9. Right: $\nu=2.4$ THz, $Q=(0.5,0,1+q_Z)$. The weak peak on the left corresponds to $(0,1+\eta,0.5)$ of domain X, the main one to $(0.5,1+\eta,0)$ of domain Y, and they define magnon modes marked $2'$ and 2 in Fig. 9. No contribution $(0.5,0,1+\zeta)$ of the domain Z is expected.

ment performed at $Q=(1.118,0,0)$ is also reported. This Q value has the same modulus as the previous ones but no low-frequency mode is expected there. The three measurements differed only by a simple sample rotation, and any anomalous contribution related to parasitic scattering or neutron shielding leakage would be present in each of them. The result demonstrates the reliability of the measurements and also provides a flat background reference for the data analysis.

Two modes are identified: a peak at $\nu=0.75$ THz, which is due to the domain contamination, and another one at $\nu=1.05$ THz, which corresponds to the gap value observed by Raman scattering by Szuszkiewicz *et al.*[58,61] A low-frequency tail is also evidenced. This tail is due to a well-known effect of the instrumental TAS resolution when a constant-Q measurement is performed inside the dispersion cone of a mode starting from zero frequency or with a gap unresolved because of the resolution of the measurement. This observation leads to the conclusion that the acoustic mode, which is doubly degenerate in the absence of anisotropy, is split in such a way that one mode is still starting from zero or a small frequency and the second one starts with a frequency gap of 1.05 THz. This is important for the characterization of the dominant anisotropy and will be discussed in Sec. V.

The low-frequency part of the spin-wave spectrum was not easy to disentangle. As there are two sets of planes, optical modes due to the interaction between sublattices are expected. Because of the weak coupling between the two sets of planes, which is a characteristic feature of the AF III-type structure, these optical modes have low frequencies. This, added to the mode superposition due to domain effects, made it particularly difficult to analyze the measured intensity. Finally the key point was to use the prediction of a spin-wave model (see the Appendix) to analyze measurements where the same domain contributions were present with different ratios. For that purpose, we performed two series of measurements, one along $Q=(0.5-q_X,0,1)$ and the other along $Q=(1,0,-0.5+q_Z)$. The choice of coordinates is such as to get a simple sample rotation between the series and thus to keep constant resolution effects such as focusing for dispersive modes.

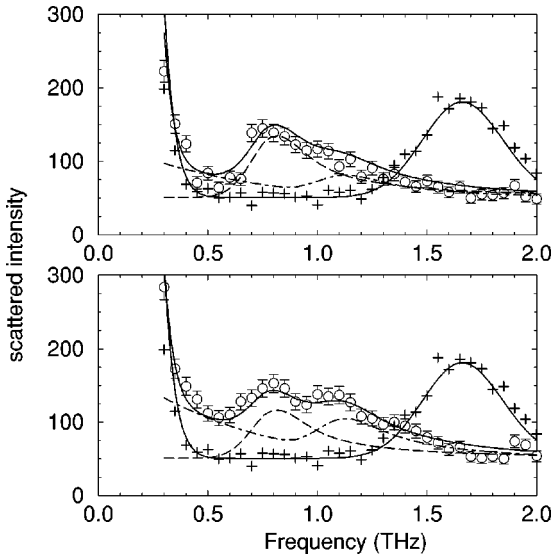

FIG. 7. Constant-Q measurements, with $k_f=2.662$ Å^{-1} at $T=15$ K : (a) open circles, $Q=(\frac{1}{2},0,1)$, Bragg center for domain X; (b) open circles, $Q=(1,0,\frac{1}{2})$, Bragg center for domain Z. In both cases the result of a measurement made after a sample rotation of 30° (+ symbols) has been added. The dot-dashed lines correspond to the calculated contributions of the domain associated with the Bragg peak, the dashed lines to those of two other domains, taking into account the domain populations and the influence of the experimental resolution on the spin-wave modes. Both the dispersion and dynamical structure factor were deduced from the analysis presented in Sec. V.

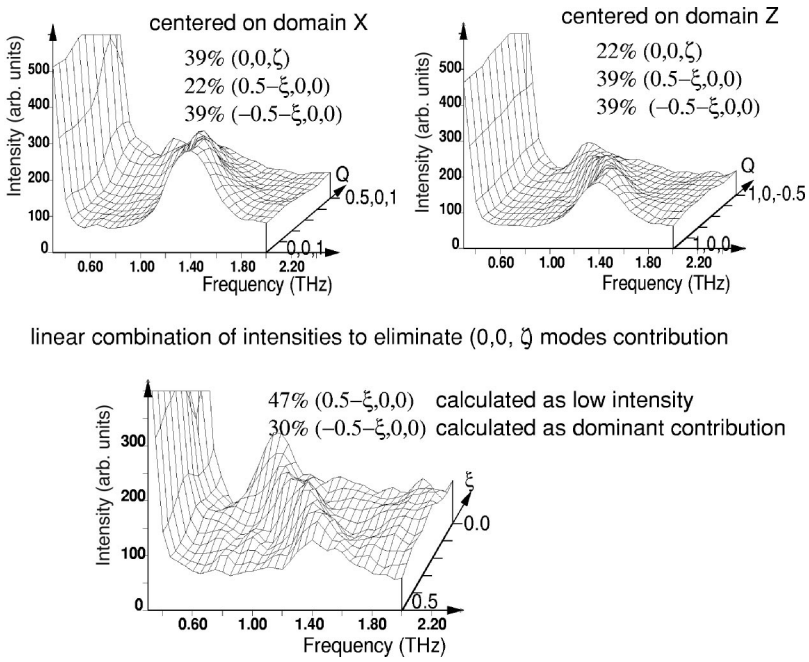

FIG. 8. Measured spin-wave cross sections as a function of wave vector and energy. Top panel: left, starting from the zone center of domain *X*; right, starting from the zone center of domain *Z*. Bottom panel: deduced contribution of the domain with vertical stacking axis, which corresponds to a low-frequency mode along the $[\xi,0,0]$ direction with $0.5<\xi<1$ measured in the *Y* domain in the Brillouin zone centered on the (110) Bragg peak.

The overall results are reported in the top panel of Fig. 8. For the sake of clarity, the data are reported with a slight smoothing, obtained by weighting each point with a contribution of its nearest neighbors. The first set of measurements is the superposition of the $(0,0,\zeta)$ mode of the domain *X* (39%), starting from the zone center $(0,1,\frac{1}{2})$, of the $(0.5-\xi,0,0)$ mode of the domain *Z* (22%), starting from the zone center (0,0,1), and of the $(-0.5-\xi,0,0)$ mode of the domain *Y* (39%), starting from the zone center (1,1,0), with ζ and ξ varying from 0 to 0.5. The second set of measurements is the superposition of an equivalent combination of modes, but with different weighting, respectively 22%, 39%, and 39%. As the spin-wave model predicts a contribution of the $(0.5-\xi,0,0)$ mode decreasing very rapidly with increasing ξ value, the direct difference (Series 1)-(Series 2) is essentially the contribution of the $(0,0,\zeta)$ mode. The linear combination of scattered intensities 0.39*(Series 1)−0.22*(Series 2) gives essentially the contribution of the $(-0.5-\xi,0,0)$ mode and is reported in the bottom panel of Fig. 8. These data were then used to go a step further in the model refinement. The final results of the data acquisition are reported in Fig. 9 together with theoretical curves, calculated according to the model presented in detail in Sec. V.

IV. TEMPERATURE DEPENDENCE

As mentioned above, the temperature dependence of a few measurements has been used to ascertain the magnetic origin of the scattering. Beyond this basic test, temperature dependence has also evidenced a strong damping effect, which was not expected since the magnetic transition is of first order. This is illustrated in Fig. 10 for a *q* value along

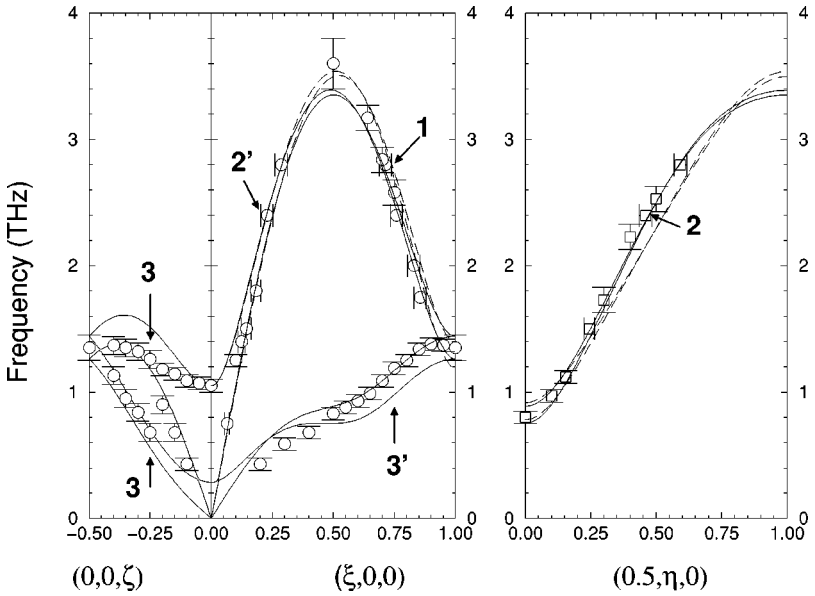

FIG. 9. Spin-wave dispersions of MnTe measured at $T\approx 15$ K. Full lines correspond to modes calculated with J_3 and J_4 interactions, dashed lines correspond to the case where they are neglected (only the high-frequency modes are shown). Points marked 1, 2, and 2′ correspond to examples presented in Fig. 6, points 3 and 3′ to those of Fig. 10.

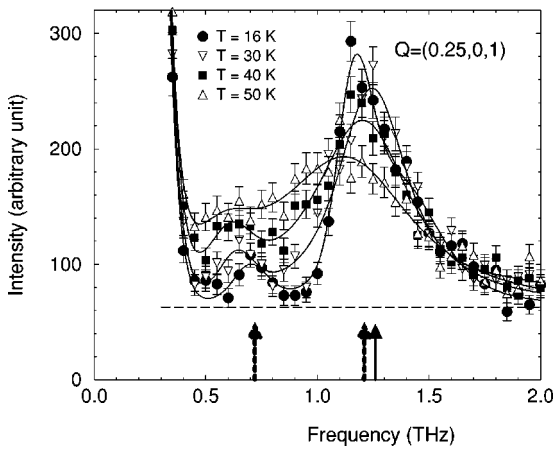

FIG. 10. Temperature dependence of the scattering measured at $Q_X=(0.25,0,1)$. The arrows show the position of modes at $T=16$ K. Peaks at 0.72 and 1.21 THz correspond to modes propagating in the $[0,0,\zeta]$ direction with $\zeta=0.25$ (marked 3 in Fig. 9), the peak at 1.26 THz is due to a domain contamination and corresponds to a mode propagating along $[\xi,0,0]$ with $\xi=0.75$ (marked $3'$ on Fig. 9).

the $[0,0,\zeta]$ direction, which has been used to obtain the lowest-frequency mode in this direction. The small peak observed at 0.72 THz at $T=16$ K is quite weak and could have been an artifact. However, an increase of temperature enhances the scattering due to the Bose thermal factor, which ensures the physical origin of the peak. It is also observed that this mode and the higher modes at about 1.25 THz become broader with increasing temperature, pointing out an important damping.

A similar observation is presented in the top panel of Fig. 11 for a measurement performed at $Q_X=(0,0,1)$. For this Q value the contributions of all domains are superimposed, which made the analysis much easier. Using a classical damped harmonic-oscillator model to describe the spin-wave mode, we obtained the temperature dependence of its frequency and damping, shown in the bottom panel of Fig. 11. The damping value at low temperature may be slightly overestimated because of the assumption of a single mode, neglecting a possible lift of the double degeneracy. The main conclusion of this analysis is that the system shows only a small renormalization of its spin-wave spectrum (which is consistent with the first-order character of the transition) but at the same time an anomalously large damping.

This kind of temperature dependence has been observed for several Q values in the present study and it had already been observed for the gap mode at $q=0$ by Raman scattering.[61] Such a behavior is not usual for an ordered magnetic system of localized spins. The standard mechanism of the transition towards a paramagnetic state is the reduction of the magnetic moment, due to the thermal population of magnons, which in turn renormalized the spin-wave spectrum in the same proportion. In the present case the transition seems rather related to a divergence of the damping, which prevents a spin deviation from propagating as a plane wave through the magnetic system, giving rise to localized defects. Possible origins of such a behavior will be discussed in Sec. V E.

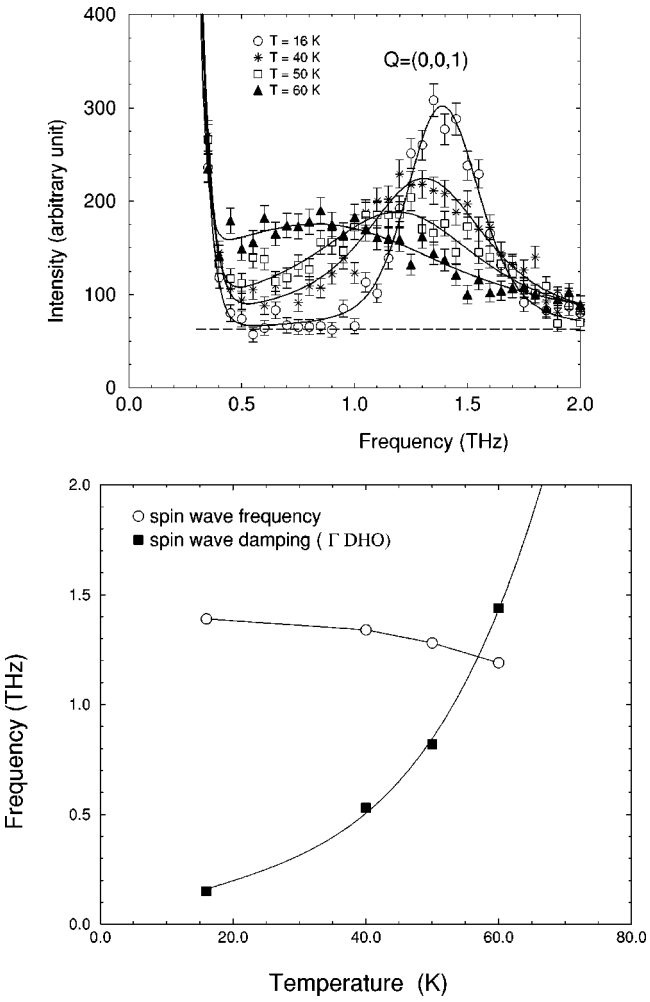

FIG. 11. Top: the scattering measured at $Q_X=(0,0,1)$ versus temperature. Bottom: temperature dependence of the frequency and damping of the spin wave in a damped harmonic-oscillator approximation.

V. DATA ANALYSIS AND DISCUSSION

The analysis of the spin-wave spectrum implies the knowledge of the ground state which defines the structural characteristics of the magnetic system and the definition of the perturbative terms of the Hamiltonian involved in the collective excitations.

We have used as a starting point the Hamiltonian defined as

$$\mathcal{H}=\sum_{lm\lambda\mu} J_{lm\lambda\mu}\vec{S}_{l\lambda}\cdot\vec{S}_{m\mu}+\sum_{l\lambda} DS_{l\lambda}^{z\,2}-h_a\sum_{l\lambda_\uparrow\lambda_\downarrow}(S_{l\lambda_\uparrow}^{w}-S_{l\lambda_\downarrow}^{w}) + \mathcal{H}_{anis}, \tag{1}$$

where l and m are cell indices, λ and μ are site indices inside the cell, and $J_{lm\lambda\mu}$ are the isotropic exchange integrals. The dominant mechanism of the exchange interaction is the superexchange mediated by Te ions and all the contributions are expected to be antiferromagnetic, which means positive values with the definition of Eq. (1). To check the importance of distant neighbors we kept exchange interactions up to the

fourth neighbors. The tetragonal distortion induces an exchange distortion between neighbors in the same AF plane or in different planes. We will account for that only for the nearest neighbors, introducing $J_1 - dJ_1$ for neigbors in adjacent planes.

The choice of the anisotropy terms is not straightforward. We know from neutron diffraction[19] that the spin direction lays within the plane perpendicular to the elongation axis of the tetragonal distortion. Therefore we used as a starting point an easy-plane anisotropy term written as $\Sigma_{l\lambda} D S^{z\,2}_{l\lambda}$. The easy magnetization axis in the AF plane is unknown and arbitrarily defined by *w*. The anisotropy needed to determine this direction is written $-h_a \Sigma_{l\lambda_\uparrow \lambda_\downarrow} (S^w_{l\lambda_\uparrow} - S^w_{l\lambda_\downarrow})$, where $\lambda_\uparrow$ and $\lambda_\downarrow$ index spins up and down.

Finally $\mathcal{H}_{anis}$ represents anisotropic exchange which is also expected, generally of the form of the Dzialoshinski-Moriya interaction $D_{DM} \Sigma_{ij} \vec{D}_{l\lambda m\mu} \cdot (\vec{S}_{l\lambda} \vec{S}_{m\mu})$.

The calculation of the spin-wave modes and of the inelastic-neutron-scattering cross sections are given in the Appendix. The comparison to experimental data is done by defining a limited set of parameters entering Eq. (1) and adjusting their numerical values to get a better agreement between calculated and measured modes. The definition of the Hamiltonian is not unique and depends on the physical assumptions used for the dominant mechanisms. The ground state itself is still debated, as the collinear arrangement of the spins in AF adjacent planes is in competition with a canted state, up to a 90° rotation, as proposed by Keffer.[45]

We have performed a comparison between experiment and calculation, starting from Eq. (1), where, at the first step, anisotropic exchange has been negelected. Then we modified the Hamiltonian to account as far as possible for the discrepancies between calculation and experiment.

For a better understanding of the relationship between the adjustable parameters and the measured spin waves, we may use the equation of the spin-wave dispersion obtained in the case of a collinear structure when anisotropy and anisotropic exchange are both neglected (see the Appendix). This yields in the [100] direction,

$$\begin{aligned}\omega^2 = 16S^2[&2(J_1 - 2J_3)(1 - \cos \pi\xi) - J_2(1 - \cos 2\pi\xi + h_a)] \\ &\times \{2J_1(1 + \cos \pi\xi) + J_2(1 + \cos 2\pi\xi) - 4J_3(1 \\ &- \cos \pi\xi) + 4J_4(1 + \cos 2\pi\xi) + h_a \pm [2(J_1 - dJ_1)(1 \\ &+ \cos \pi\xi) + 2J_3(\cos \pi\xi + \cos 2\pi\xi)]\}. \qquad (2)\end{aligned}$$

It may easily be seen that i) the velocity of the acoustic branch is dominated by J_1, (ii) at $q=(0.5,0,0)$ the frequency of the lowest mode is proportional to dJ_1 and that of the highest one proportional to J_1, (iii) the zone-boundary frequency at $q=(1,0,0)$ is given by $\omega^2 = 128S^2(J_1 - 2J_3)(J_2 - 4J_3 + 4J_4)$. We also know that the gap induced at $q=0$ by a planar anisotropy is proportional to DJ_1. Hence J_1 and D are essentially determined by the gap at $q=0$, the slope of the acoustic mode, and its maximum frequency in the [100] direction. The zone-boundary mode clearly imposes a strong linear constraint between J_2, J_3, and J_4, while the effects of individual contributions are reflected in the q dependence of the spin-wave dispersion. Finally, we see that the exchange distortion dJ_1 prevents a structural instability at $q=(0.5,0,0)$ (as does h_a when introduced). Hence the determination of dJ_1 will be very sensitive to the lowest frequency at this q value and will be strongly affected by the assumption on the anisotropy terms.

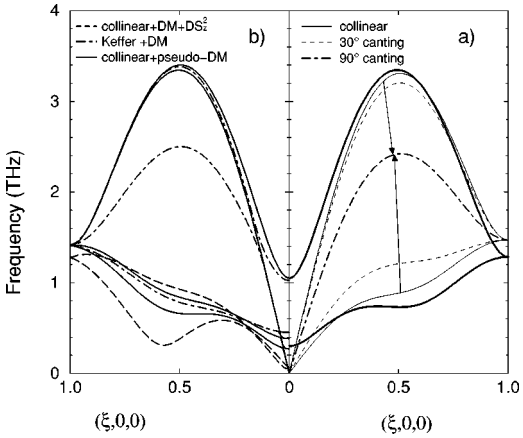

FIG. 12. (a) Effects of a canting of the magnetic structure on the spin-wave dispersion in the $[\xi,0,0]$ direction. The thick lines are branches not affected by the canting. Arrows indicate the moves of branches affected by the canting, starting from the collinear structure to the Keffer structure. The dispersions have been calculated with the parameters used in Fig. 9. (b) Effects of an anisotropic exchange interaction between nearest neighbors. See details in the text of Sec. V D.

The calculation performed with the assumption of a canted structure shows that the highest and lowest modes stay at the same values as in the collinear case, so that the previous considerations are still valid.

A. Collinearity

A preliminary question for the spin-wave analysis is the nature of the ground state, as there is an uncertainty on the collinearity of the structure. Therefore we have performed a model calculation, where only isotropic exchange interactions and planar single-site anisotropy have been used, to visualize the evolution of the spin-wave modes when introducing a canting angle between spins of adjacent AF planes. Such a canting of the structure only affects the modes not sensitive to the planar anisotropy, which start linearly from the zone center. The acoustic like mode (upper branch) and the optical-like mode (lower branch) move towards each other to merge in a degenerate mode in the case of a 90° rotation, as illustrated on Fig. 12(a). The calculation of the inelastic-neutron-scattering cross section shows that in the conditions of the present experiment all the modes would be observable.

A qualitative comparison with the experimental results reported in Fig. 9 clearly excludes the Keffer structure. The experimental evidence of a small canting should be a broadening of the lowest mode in the vicinity of $q=(0.5,0,0)$, because a canting enhances the splitting at that point. The analysis of the mode at $q=(0.5,0,0)$, illustrated in Fig. 7, and of the segment $q=(\xi,0,0), 0.5<\xi<1$, reported in the

bottom panel of Fig. 8, did not need any intrinsic broadening, the linewidth of the modes being accounted for by the experimental resolution. This is in favor of a collinear (or very weakly canted) structure. We have also checked that the inclusion of anisotropic exchange terms did not change the main features of the dispersion and could not affect the conclusion.

B. Anisotropy

The experimental observations at the zone center are consistent with the assumption of a dominant planar anisotropy. Indeed such a term removes the twofold degeneracy of the acoustic branch and yields a branch with a gap, when the other branch still departs linearly from the zone center. An axial anisotropy would induce a gap without affecting the degeneracy. No small frequency gap could be detected in our measurements, which gives an upper limit of ≈ 0.3 THz for a possible gap because of the experimental resolution. As a consequence we kept $h_a = 0$ for further analysis.

However the use of a single-site term to describe the planar anisotropy has the effect of propagating a large mode splitting all along the Brillouin zone. Such a splitting would have been observed on the low-frequency modes, even with the limited resolution of our measurements. This is likely a hint that a more sophisticated description of the anisotropy is needed for a better description of the magnetic system. We will come back to this point in Sec. V D.

C. Exchange

Many previous works used J_1 and J_2 as the dominant exchange interactions, but the importance of J_3 and J_4 has become an important issue. We checked both assumptions, adjusting the parameters to obtain the best fit with the experimental data. This was done by minimizing the reduced χ^2, defined as $\chi^2 = 1/(N-n)\Sigma_{i=1,N}[y_{\mathrm{calc}}(i) - y_{\mathrm{exp}}(i)]^2/\Delta y(i)^2$, where N is the number of experimental values (we used 51 experimental data) and n is the number of adjusted parameters (up to 6, with the neglect of h_a). With only J_1, dJ_1, J_2, and D we obtained (in units of kelvin) $J_1 = 6.34(5)$, $dJ_1 = 0.59(2)$, $J_2 = 0.63(2)$, and $D = 1.03(2)$ with a χ^2 value of 4.54, while adding J_3 and J_4 we obtained $J_1 = 5.71(7)$, $dJ_1 = 0.52(2)$, $J_2 = 0.08(5)$, $J_3 = 0.00(1)$, $J_4 = 0.18(2)$, and $D = 1.12(2)$ with a χ^2 value of 1.97. The improvement of the χ^2 is significant and is mainly due to a better description of the high-frequency modes in the $[\xi,0,0]$ and $[0.5,\eta,0]$ directions as shown in Fig. 9. These high-frequency modes are not much affected by the anisotropy term and thus the values obtained for the exchange interactions do not depend on the description of this anisotropy. We have already mentioned the linear correlation imposed by the value of the mode at the zone boundary. This means that the uncertainties on the estimated values are correlated in the same way. As J_3 is found almost negligible, it means that the sum $J_2 + 4J_4$ should be kept nearly constant when deviating from the optimal values given by the fit. This also explains the very large change of the J_2 value when introducing J_3 and J_4. The dJ_1/J_1 ratio is found $\approx 9\%$ in both cases, which seems a value too high to be realistic. This likely points out the limit of the used Hamiltonian.

D. Anisotropic exchange

This step of the data analysis provided us with a set of exchange interactions stable as regards the assumption on the anisotropy term. It also suggested that the anisotropy was not well described, as pointed out by the very large splitting of the low-frequency modes and an obviously too high value of dJ_1/J_1. Therefore we considered the effects on the spin-wave spectrum of the introduction of anisotropic exchange interactions, adding a Dzialoshinski-Moriya term to the Hamiltonian. But forcing such a term on the collinear structure does not decrease the value of the single-site planar anisotropy and has the effect of enhancing the splitting of the low-frequency modes near $q = (0.5,0,0)$, as illustrated by the dashed lines in Fig. 12(b) (only low-frequency modes are reported). This could even lead to $\omega^2 < 0$ values, reflecting the instability of the collinear structure as regards such a term. To compensate for this effect, we would then need a large h_a or a still larger dJ_1/J_1 value. So such a DM term has to be discarded.

Nevertheless the existence of a canted state has been ascertained in diluted systems[72] as a step towards a spin-glass state and related to the high frustration of the AF III structure. The tendency of a DM interaction to induce spin rotation is well in agreement with such a behavior. Without questioning the previous conclusion on the collinearity of the magnetic structure, we have checked the consequences of a DM term in the case of a Keffer structure. The result is displayed by the dot-dashed lines in Fig. 12(b). The doubly degenerate mode specific to this structure and incompatible with our data does not change, but the effects on the two other modes are in a very good qualitative agreement with what we are looking for. With D_{DM} corresponding to $\approx 6\%$ of J_1, the correct gap at the zone center is reproduced without additional single-site anisotropy and the frequency of the lower mode at $q = (0.5,0,0)$ is enhanced, allowing thus a realistic value of $dJ_1/J_1 = 2\%$.

A continuity argument may be used to assert that a DM term on a weakly canted structure would only induce small effects. Then, coming back to the collinear structure, we directly injected into the development of the Hamiltonian the correcting terms derived from a DM interaction in the Keffer structure. Doing that, we are unable to write the exact expression for the corresponding exchange term, because the correction so-obtained contains only the two-operator parts of its development in the Holstein-Primakoff approximation.[73] Thus the physical meaning of such a term remains undefined. Nevertheless, the effects of such a term in the collinear case have still the right properties. With a weight of $\approx 4\%$ of J_1 and $dJ_1/J_1 = 5\%$, we obtain the dispersions drawn in full lines in Fig. 12(b).

The validity of such a procedure is not ascertained, but the weight of the correction needed to get the desired effects is in a very realistic range, when compared to estimations by Larson and Ehrenreich[47] of the importance of anisotropic exchange in ZB MnTe-based systems.

TABLE I. Comparison of experimental and theoretical values of exchange integrals. Values of the nearest-neighbor exchange J_1 are given in kelvin and more distant neighbor interactions are given relative to J_1. The first two columns are experimental data for highly diluted $Zn_{1-x}Mn_xTe$ (Refs. 39 and 40) and $Cd_{1-x}Mn_xTe$ (Ref. 41), respectively, then three theoretical predictions for $Cd_{1-x}Mn_xTe$ (Ref. 36) and pure ZB MnTe (Refs. 37 and 38) are given. The last column corresponds to the present determination.

	Experiment		Theory			This work
	Refs. 39 and 40	Ref. 41	Ref. 36	Ref. 37	Ref. 38	
J_1 (K)	9	6.1	11.1	9.3	7.72	5.71(7)
J_2/J_1	0.022	0.010	0.006	0.034	0.054	0.014(7)
J_3/J_1	0.018	0.030	0.024	0.017	0.001	0.000(5)
J_4/J_1	0.057	0.064	0.065	0.041	0.003	0.032(6)

Therefore we believe that this points out the existence of an incipient anisotropic exchange mechanism involved in the definition of the system Hamiltonian, compatible with the existence of the canted structure in DMS's.

It is also worthwhile to notice that the various dispersions reported in Fig. 12 are obtained with the set of isotropic exchange integrals deduced from the analysis reported in Sec. V C, with at most a slight deviation within the error bars.

E. Discussion

From the analysis of our experimental data, we deduced exchange integrals up to the fourth neighbors. Due to the strong linear correlation between J_2, J_3, and J_4, the uncertainties given by the best fit to experimental data are also correlated, following approximately the relation $\Delta J_2 - 4\Delta J_3 + 4\Delta J_4 = 0$. More experimental data in less symmetric directions would have been needed to get a better definition of these interactions, which was impossible due to the experimental difficulties mentioned in Sec. III. Nevertheless the values obtained from our analysis are stable as regards the various assumptions made on the anisotropy terms and on the collinearity of the structure. The main conclusions are that J_4 is at least as important as J_2, and that J_3 is almost negligible. This corroborates the importance of the bridging mechanism of Mn by Te ions prior to the direct distance between neighbors. The comparison with other experimental and theoretical values of exchange integrals is summarized in Table I.

The value of J_1 deduced from our measurements is noticeably below all other determinations or predictions. This may be due to the fact that we are dealing with a pure system: the tetragonal distortion associated with the magnetic transition may affect the superexchange mechanism and the absence of disorder prevents perturbations of the electronic characteristics of the system and of the exchange mechanism linked to them, such as the Bloembergen-Rowland interaction.[74]

The same kind of arguments may be invoked to explain the differences with the estimations of J_2, J_3, and J_4 obtained on highly diluted systems. Nevertheless the overall conclusions on the relative importance of distant neighbors are quite similar.

The complex behavior of the lower modes near $q = (0.5,0,0)$, depending on exchange distortion dJ_1 and/or anisotropic exchange, prevents a precise determination of dJ_1. The value of 9% obtained when a single-site planar anisotropy and isotropic exchanges are used in the system Hamiltonian, is unrealistic as regards what may be deduced from the geometrical dependence of the superexchange.[35,52–54] In the same way, the single-site planar anisotropy term of 1.1 K used to reproduce the zone-center gap is certainly a very high value. To get rid of these discrepancies we have to introduce additional terms in the Hamiltonian. A DM interaction would be efficient in the Keffer state, but another form is needed to be compatible with a collinear or weakly canted structure. We cannot deduce from the analysis of our data the literal expression of such a term nor the underlying exchange mechanism, which is likely related to the vicinity of a canted structure, favored by disorder as revealed by the substitution of Mn by Cd.[72]

This analysis was done on low-temperature data. But we have also observed a very peculiar temperature dependence of the spin-wave spectrum, with a significant damping well below the transition temperature and strongly increasing with temperature, while at the same time the frequencies of the modes evolve in a more common way with a slight decrease. This behavior is not expected for a transition towards a paramagnetic state in an insulating system. The usual origin of the damping in this class of magnetic systems is due to magnon-magnon interaction and becomes effective in the vicinity of the transition. Furthermore, in the present case the transition is of the first order, which should still decrease this effect. A relevant comparison may be found in the evolution of the spin waves in MnO. In that case, Mn ions also form a fcc lattice and the system undergoes a first-order transition towards an AF state of type II, associated with a trigonal distortion. Spin-wave measurements[75,76] evidenced a decrease of the spin-wave frequencies with no strong damping when approaching T_N. In the present study, we could only investigate the temperature dependence of the spin waves for a few q values, as illustrated in Figs. 10 and 11, but this is enough to state that this abnormal damping is not specific of a particular q. A complementary information comes from Raman-scattering measurements on ZB MnTe, where the zone-center mode has been followed with increasing temperature, revealing a small decrease of its frequency,[61] but the observed damping, which also increases rapidly near T_N, keeps small absolute values in comparison with the mode frequency.[77] So we can also state that there is a q dependence of the spin-wave damping.

This kind of damping could be due to an interaction between spin-wave modes and ''other modes'' of the system, related to structural or electronic characteristics of the material, or to a very large anharmonicity.

Because of the quenching of the Mn orbital moment we cannot expect a strong magnon-phonon coupling related to spin-orbit coupling. The usual interaction between magnetic and structural dynamical properties in insulating systems is due to the fact that the spins are linked to ions, and, in the case of magnetic superexchanges, that the exchange is mediated by intermediate ions. So the lattice vibrations induce a modulation of the spin positions and also of the exchange interactions. This should lead to a q-dependent broadening of the spin-wave modes. This mechanism is usually considered as giving rise to only small effects. Would ZB MnTe be an exception?

Another suggestion would be that the anisotropic exchange term, which is needed to replace the single-site planar anisotropy of our description, would involve four-operator terms, such as biquadratic exchange,[2] giving rise to a thermal dependence of this contribution. This would be in accordance with the vicinity of a canted state in the phase diagram of the system and would affect preferentially the optical modes which reflect the sublattice interplay.

Evaluating the effects of such a coupling is beyond the scope of the present paper. But most of the discrepancies with standard models, pointed out by our analysis, could have a common origin in the very strong correlation between structural and magnetic properties, either via the definition of the magnetic exchange interactions or via any kind of coupling between magnons and lattice vibrations.

VI. CONCLUSIONS

The spin-wave spectrum of MnTe has been obtained by inelastic neutron scattering on a MBE-grown sample with ZB structure. The salient features of the spin-wave dispersion exclude the Keffer structure and favor a collinear or only weakly canted structure. The accuracy of the measurements was high enough to analyze the interactions up to fourth neighbors. The numerical determination of the exchange integrals is nearly independent of the assumptions made on the anisotropy of the system and the importance of distant neighbors is well confirmed and qualitatively supports theoretical predictions of exchange interaction models or *ab initio* calculations. Our determination of the nearest-neighbor exchange J_1 is at the lower limit or even below the common extrapolation based on diluted MnTe magnetic systems.

The assumption of a single-site planar anisotropy allows to account for the observed lift of the degeneracy near the zone center, but has the consequence of propagating all along the Brillouin zone a splitting of the spin-wave branches, which is not observed. This discrepancy and the very high value of the exchange distortion, $dJ_1/J_1 \approx 9\%$, points out the necessity of a more specific intersite anisotropy term. The Dzialoshinski-Moriya anisotropic exchange between nearest neighbors, which is usually referred to, is inefficient to account for our experimental data with the constraint of a collinear structure. A correcting term deduced from the development in the Holstein-Primakoff approximation of a DM term applied to a Keffer structure has been injected in the calculation of the spin waves of the collinear system. The main features of the experiment are thus reproduced, with a weight of this term corresponding to $\approx 4\%$ of J_1. This can only be considered as a strong indication that a specific anisotropic exchange would be able to account for the experimental observation. But the literal expression of such a term is still to be found.

An anomalous damping of the spin waves has been observed, which reveals a strong perturbation of the collective magnetic modes. This could be due to the high anharmonicity of the system or to a dynamical modulation of the exchange interactions. We can unfortunately not assert that there is a common explanation of this temperature dependence and of the need of an unusual anisotropic exchange.

The experimental study presented in this paper should provide a set of data useful for quantitative comparison with further theoretical models. On another hand, such a determination of spin-wave branches in a MBE-grown sample may also be considered as a step towards similar measurements performed on quantum magnetic structures obtained via epitaxial growth, such as, for instance, superlattices made of MnTe and ZnTe thin layers. The same kind of measurements may indeed be undertaken on samples with a typical thickness of 1 μm when the magnetic moment per unit cell is of same order as that of Mn^{2+} in this study.

ACKNOWLEDGMENTS

We would like to express our gratitude to Professor J. Kossut for his continuous interest in the present studies as well as for his encouragement. Thanks are also due to J. Domagała for his kind help in the layer structure characterization. One of us (T.W.) acknowledges the hospitality of the University of Notre Dame, where final stages of work on this manuscript were done. This study has benefited from financial support within the frame of a POLONIUM project, a cooperation between CNRS (France) and the Polish Academy of Sciences (Poland). The work was also supported in part by the Committee for Scientific Research (Poland) through Grant No. PBZ/KBN/044/P03/2001, within European Community program ICA1-CT-2000-70018 (Centre of Excellence CELDIS) and by the European Commission through the Access to Research Infrastructures Action of the Improving Human Potential Programme (Contract No. HPRI-CT-1999-00032).

APPENDIX

To find the eigenvalues of Eq. (1), we have to make some assumption on the magnetic structure. The simplest one is to suppose that the structure is collinear. In this case we may specify up and down spins by defining $\vec{S}_{l\lambda}$ and $\vec{T}_{m\mu}$ such as

$$S^u_{m\mu} = T^u_{m\mu},$$

$$S^v_{m\mu} = -T^v_{m\mu},$$

$$S^w_{m\mu} = -T^w_{m\mu}$$

and

$$S^+_{m\mu}=T^-_{m\mu},$$

$$S^-_{m\mu}=T^+_{m\mu},$$

where S^u,S^v,S^w are the spin components, w labels the spin direction, which is supposed to be within the xy plane of a given domain, u,v is an arbitrary choice to define the transverse components of the spin. We then use a Holstein-Primakoff approximation[73]

$$S^+_{l\lambda}=\sqrt{2S}a_{l\lambda},$$

$$S^-_{l\lambda}=\sqrt{2S}a^\dagger_{l\lambda},$$

$$S^w_{l\lambda}=S-a^\dagger_{l\lambda}a_{l\lambda},$$

and

$$T^+_{m\mu}=\sqrt{2S}b^\dagger_{m\mu},$$

$$T^-_{m\mu}=\sqrt{2S}b_{m\mu},$$

$$T^w_{m\mu}=-S+b^\dagger_{m\mu}b_{m\mu},$$

where $a_{l\lambda}$, $a^\dagger_{l\lambda}$, $b_{m\mu}$, and $b^+_{m\mu}$ are boson operators creating or annihilating a spin-1/2 deviation at sites $l\lambda$ or $m\mu$. Then we write the Fourier transforms

$$a_{l\lambda}=\frac{1}{\sqrt{N}}\sum_k \exp(i\vec{k}\cdot\vec{r}_{l\lambda})a_\lambda(\vec{k}),$$

$$a^\dagger_{l\lambda}=\frac{1}{\sqrt{N}}\sum_k \exp(-i\vec{k}\cdot\vec{r}_{l\lambda})a^\dagger_\lambda(\vec{k})$$

and

$$b_{m\mu}=\frac{1}{\sqrt{N}}\sum_k \exp(-i\vec{k}\cdot\vec{r}_{m\mu})b_\mu(\vec{k}),$$

$$b^\dagger_{m\mu}=\frac{1}{\sqrt{N}}\sum_k \exp(i\vec{k}\cdot\vec{r}_{m\mu})b^\dagger_\mu(\vec{k}),$$

where N is the number of cells. The operators obey the commutation rules $[a_\lambda(\vec{k}),a^\dagger_{\lambda'}(\vec{k}')]=\delta_{\lambda\lambda'}\delta_{\vec{k}\vec{k}'}$ and $[b_\mu(\vec{k}),b^\dagger_{\mu'}(\vec{k}')]=\delta_{\mu\mu'}\delta_{\vec{k}\vec{k}'}$.

Each term of the Hamiltonian may be written as a function of these operators, using for the planar anisotropy the relation[78]

$$(S^z)^2=-\tfrac{1}{4}[(S^+)^2+S(S^-)^2-2S-2S^-S^+],$$

where z labels the direction perpendicular to the easy plane. Keeping only terms with two operators, this yields $\mathcal{H}=\Sigma_k H_k$, where H_k is a bilinear form of the operators. A linear transformation is then needed to get the Hamiltonian in its diagonal form. We introduce four operators α_i, with

$$\begin{aligned}\alpha_i(k)=&x_{i1}a_1(k)+x_{i2}a_2(k)+x_{i3}b^\dagger_3(k)+x_{i4}b^\dagger_4(k)\\&+x_{i5}a^\dagger_1(-k)+x_{i6}a^\dagger_2(-k)+x_{i7}b_3(-k)\\&+x_{i8}b_4(-k),\end{aligned}$$

which obey the commutation rule $[\alpha_i(\vec{k}),\alpha^\dagger_j(\vec{k}')]=\delta_{ij}\delta_{kk'}$ and such that $[\alpha_i(k),\mathcal{H}]=\omega_i(k)\alpha_i(k)$, where $\omega_i(k)$ are the eigenvalues of the Hamiltonian. The eigenvalues are the values of ω that give a zero value of the determinant

$$\begin{vmatrix}
a-\omega & b & c & -b^* & d & 0 & 0 & 0\\
b^* & a-\omega & -b & c & 0 & d & 0 & 0\\
-c & b^* & -a-\omega & -b & 0 & 0 & -d & 0\\
b & -c & -b^* & -a-\omega & 0 & 0 & 0 & -d\\
-d & 0 & 0 & 0 & -a-\omega & -b & -c & b^*\\
0 & -d & 0 & 0 & -b^* & -a-\omega & b & -c\\
0 & 0 & d & 0 & c & -b^* & a-\omega & b\\
0 & 0 & 0 & d & -b & c & b^* & a-\omega
\end{vmatrix},$$

where

$$\begin{aligned}a=&z_{13}+z_{14}-z_{12}+\gamma'_{11}-z'_{11}+z'_{13}+DS+h_a+\gamma''_{11}-z''_{11}+z''_{14}\\&-z''_{12}+\gamma'''_{11}-z'''_{11}+z'''_{13},\end{aligned}$$

$$b=\gamma_{12}+\gamma''_{12},$$

$$c=-\gamma_{13}-\gamma'_{13}-\gamma'''_{13},$$

and

$$d=DS,$$

with $\gamma_{ij}=2S\Sigma_{ij}J_{ij}\exp(i\vec{k}\cdot\vec{d}_{ij})$ and $z_{ij}=\gamma_{ij}(0)$. Here, $\vec{d}_{ij}$ is a vector joining site i to site j, $\gamma'_{ij},\gamma''_{ij},\gamma'''_{ij}$ and $z'_{ij},z''_{ij},z'''_{ij}$ are

used for second, third, and fourth neighbors.

Because of the tetragonal distortion we take for the nearest neighbors $J_{13}=J_{24}=J_1$ and $J_{12}=J_{14}=J_1-dJ_1$. This yields

$$\gamma_{12}=4(J_1-dJ_1)S[\cos\pi k_\zeta(\cos\pi k_\xi+\cos\pi k_\eta)+i\sin\pi k_\zeta(\cos\pi k_\xi-\cos\pi k_\eta)],$$

$$\gamma_{13}=8J_1S\cos\pi k_\xi\cos\pi k_\eta,$$

$$\gamma'_{11}=4J_2S[\cos(2\pi k_\xi)+\cos(2\pi k_\eta)],$$

$$\gamma'_{13}=4J_2S\cos 2\pi k_\zeta$$

$$\gamma''_{11}=16J_3S\cos(2\pi k_\zeta)\cos\pi k_\xi\cos\pi k_\eta,$$

$$\gamma''_{12}=8J_3S[\exp(i\pi k_\zeta)\cos\pi k_\xi\cos(2\pi k_\eta)+\exp(-i\pi k_\zeta)\cos(2\pi k_\xi)\cos\pi k_\eta],$$

$$\gamma'''_{11}=8J_4S\cos(2\pi k_\xi)\cos(2\pi k_\eta),$$

$$\gamma'''_{13}=8J_4S\cos(2\pi k_\zeta)[\cos(2\pi k_\xi)+\cos(2\pi k_\eta)].$$

Solving the equation, we get eight eigenvalues, corresponding to $\pm\omega_i(k)$, which means four dispersion curves. With no anisotropy, this would correspond to two doubly degenerate branches, classically an acoustic mode, dispersing linearly from zero frequency near the zone center, and an optical mode. In fact in the present case both modes start from zero frequency at the zone center, because in the long-wavelength limit the two sublattices are independent, as mentioned in Sec. II B. An axial anisotropy introduces a frequency gap but does not lift the degeneracy. This degeneracy is only removed by a planar anisotropy. When the planar anisotropy term is neglected, the equation giving the two degenerate modes is $\omega^2=(a+c)(a-c\pm 2b)$. This is used in Sec. V to get Eq. (2).

To disentangle the experimental data we also needed to calculate the neutron-scattering cross section. Following Lovesey,[78] this is done starting from the general formula

$$S(\vec{Q},\omega)\propto\sum_{\alpha,\beta}(\delta_{\alpha,\beta}-\tilde{Q}_\alpha\tilde{Q}_\beta)\int dt\,\exp(-i\omega t)\times\langle\hat{X}^\alpha_Q(0)\hat{X}^\beta_{-Q}(t)\rangle$$

with $\alpha,\beta=\xi,\eta,\zeta$ and

$$\hat{X}^\alpha_Q=\sum_{l\lambda}\frac{1}{2}g_\lambda F_\lambda(\vec{Q})\exp[-W_\lambda(\vec{Q})]\exp\{-i\vec{Q}\cdot(\vec{l}+\vec{\lambda})\}\hat{S}^\alpha_{l\lambda}.$$

Here $\tilde{Q}$ is the unitary vector of the total momentum transfer, F_λ is the magnetic form factor of the Mn^{2+} ion, and W_λ is its partial Debye-Waller factor, related to thermal motions. For a collinear magnetic structure only the terms reduced as $\hat{X}^+$ and $\hat{X}^-$ are meaningful. Using the same approximation as before, with a_λ and $b^\dagger_\mu$ we get

$$S(\vec{Q},\omega)\propto(1+\tilde{Q}^2_\zeta)\sum_\tau\delta(\vec{Q}-\vec{q}-\vec{\tau})\sum_{\lambda\lambda'}\frac{1}{2}g_\lambda F_\lambda(\vec{Q})\times\exp[-W_\lambda(\vec{Q})]\frac{1}{2}g_{\lambda'}F_{\lambda'}(\vec{Q})\exp[-W_{\lambda'}(\vec{Q})]\times\exp[-i\vec{\tau}(\vec{\lambda}-\vec{\lambda}')]\langle a_\lambda(\vec{q})a^\dagger_{\lambda'}(\vec{q})\rangle.$$

By expanding $a_\lambda(\vec{q})$ as $a_\lambda(\vec{q})=\Sigma_j t_{\lambda j}\alpha_j$ and taking into account that $\langle\alpha_j(\vec{q})\alpha^\dagger_j(\vec{q})\rangle=n(\omega(\vec{q}),T)+1$, where $n(\omega(\vec{q}),T)$ is the thermal population of a boson mode, we get

$$S(\vec{Q},\omega)\propto(1+\tilde{Q}^2_\zeta)\sum_{\vec{\tau}}\delta(\vec{Q}-\vec{q}-\vec{\tau})\times\sum_j\left|\sum_\lambda\exp(-\vec{\tau}\cdot\vec{\lambda})t_{\lambda j}(\vec{q})\right|^2\times[n(\omega_j(\vec{q}),T)+1]\delta(\omega-\omega_j(\vec{q}))$$

which may be simplified because $\vec{Q}=\vec{\tau}+\vec{q}$ and $t_{\lambda j}(\vec{Q})=\exp(-\vec{\tau}\cdot\vec{\lambda})t_{\lambda j}(\vec{q})$, and $\omega_j(\vec{Q})=\omega_j(\vec{q})$.

All previous calculations are based upon the assumption of a collinear structure. In order to account for a noncollinear structure with a spin rotation of 90° between the two sublattices, we have to change the definition of spins 2 and 4 of the second sublattice. This is done by defining $\vec{S}'_2$ as

$$S'^u_{2m\mu}=S^u_{2m\mu},$$

$$S'^v_{2m\mu}=-S^w_{2m\mu},$$

$$S'^w_{2m\mu}=S^v_{2m\mu}$$

and the equivalent for $\vec{S}'_4$.

Contributions derived from $\vec{S}_1\cdot\vec{S}'_2$, which were $\gamma_{12}a_1a^\dagger_2+\gamma^*_{12}a^\dagger_1a_2-z_{12}(a_1a^\dagger_1+a_2a^\dagger_2)$ with the collinear structure, are now $1/2\{\gamma_{12}(a_1a^\dagger_2+a_1a'_2)+\gamma^*_{12}(a^\dagger_1a_2+a^\dagger_1a'^\dagger_2)\}$, which modifies the determinant yielding the eigenvalues. The calculation of the neutron-scattering cross section follows the same derivation as reported above, with the complication that we have no longer the factorization of the orientation term $1+\tilde{Q}^2_\zeta$.

To check the effect of a Dzialoshinski-Moriya term between nearest neighbors $D_{DM}\Sigma_{ij}\vec{D}_{ij}\cdot\vec{S}_i\vec{S}_j$, we used the fact that for neighbors ij with $\vec{r}_{ij}=(\frac{1}{2},\frac{1}{2},0)$ we have $\vec{D}_{ij}=(1/\sqrt{2},-1/\sqrt{2},0)$ and $\vec{D}_{ji}=-\vec{D}_{ij}$ and equivalent relations by symmetry (see Ref. 47). Only two-operator terms of the development in the Holstein-Primakoff approximation are kept, then Fourier transformed. This gave the $\vec{q}$ dependence of the anisotropic exchange generated by the coupling.

*Email address: hennion@llb.saclay.cea.fr
†Email address: szusz@ifpan.edu.pl
‡Present address: University of Notre Dame, Notre Dame, Indiana 46556.

[1] P.W. Anderson, Phys. Rev. **115**, 2 (1959).
[2] P. W. Anderson, in *Solid State Physics*, edited by F. Seitz and D. Turnbull (Academic Press, New York, 1963), Vol. 14, p. 99.
[3] B.E. Larson, K.C. Haas, H. Ehrenreich, and A.E.C. Carlsson, Solid State Commun. **56**, 347 (1985).
[4] J. Spałek, A. Lewicki, Z. Tarnawski, J.K. Furdyna, R.R. Galazka, and Z. Obuszko, Phys. Rev. B **33**, 3407 (1986).
[5] W.J.M. de Jonge, A. Twardowski, and C.J.M. Denissen, in *Diluted Magnetic (Semimagnetic) Semiconductors*, edited by R. L. Aggarwal, J. K. Furdyna, and S. von Molnar, Mater. Res. Soc. Symp. Proc. No. 89 (Materials Research Society, Pittsburgh, 1987), p. 153.
[6] A. Lewicki, J. Spałek, J.K. Furdyna, and R.R. Galazka, Phys. Rev. B **37**, 1860 (1988).
[7] B.E. Larson, K.C. Haas, H. Ehrenreich, and A.E. Carlsson, Phys. Rev. B **37**, 4137 (1988).
[8] R.R. Galazka, S. Nagata, and P.H. Keesom, Phys. Rev. B **22**, 3344 (1980).
[9] M. Escorne, A. Mauger, R. Triboulet, and J.L. Tholence, Physica B & C **107**, 309 (1981).
[10] S. Oseroff, Phys. Rev. B **25**, 6584 (1982).
[11] S.P. McAlister, J.K. Furdyna, and W. Giriat, Phys. Rev. B **29**, 1310 (1984).
[12] J.K. Furdyna and N. Samarth, J. Appl. Phys. **61**, 3526 (1987).
[13] M.E. Schlesinger, J. Phase Equilib. **19**, 591 (1998).
[14] R. R. Galazka, J. Kossut, and T. Story, in *Numerical Data and Functional Relationships in Science and Technology,* edited by O. Madelung, U. Rossler, and M. Schulz, Landolt-Börnstein, New Series, Group III, Vol. 41, Pt. b (Springer-Verlag, Berlin, 1999), p. 647.
[15] S.M. Durbin, J. Han Sungki, O.M. Kobayashi, D.R. Menke, R.L. Gunshor, Q. Fu, N. Pelenakos, A.V. Nurmikko, D. Li, J. Gosvales, and N. Otsuka, Appl. Phys. Lett. **55**, 2087 (1989).
[16] P. Kłosowski, T.M. Giebultowicz, J.J. Rhyne, N. Samarth, H. Luo, and J.K. Furdyna, J. Appl. Phys. **70**, 6221 (1991).
[17] P. Kłosowski, T.M. Giebultowicz, N. Samarth, H. Luo, J.K. Furdyna, and J.J. Rhyne, Physica B **180/181**, 114 (1992).
[18] K. Ando, K. Takahashi, and T. Okuda, J. Magn. Magn. Mater. **104-107**, 993 (1992).
[19] T.M. Giebultowicz, P. Kłosowski, N. Samarth, H. Luo, J.K. Furdyna, and J.J. Rhyne, Phys. Rev. B **48**, 12 817 (1993).
[20] M. Sawicki, S. Kolesnik, T. Wojtowicz, G. Karczewski, E. Janik, M. Kutrowski, A. Zakrzewski, T. Dietl, and J. Kossut, Superlattices Microstruct. **15**, 475 (1994).
[21] J. Pietruczanis, W. Mac, A. Twardowski, G. Karczewski, A. Zakrzewski, E. Janik, T. Wojtowicz, and J. Kossut, Mater. Sci. Forum **182/184**, 687 (1994).
[22] K. Ando and H. Akinaga, J. Magn. Magn. Mater. **140-144**, 2029 (1995).
[23] A. Stachow-Wojcik, W. Mac, A. Twardowski, G. Karczewski, E. Janik, T. Wojtowicz, J. Kossut, and E. Dynowska, Phys. Status Solidi A **177**, 555 (2000).
[24] T.M. Giebultowicz, H. Kepa, B. Buras, K. Clausen, and R.R. Galazka, Solid State Commun. **40**, 499 (1981).
[25] T.M. Giebultowicz, B. Lebech, B. Buras, W. Minor, H. Kepa, and R.R. Galazka, J. Appl. Phys. **55**, 2305 (1984).
[26] T.M. Holden, G. Dolling, V.F. Sears, J.K. Furdyna, and W. Giriat, Phys. Rev. B **26**, 5074 (1982).
[27] G. Dolling, T.M. Holden, V.F. Sears, J.K. Furdyna, and W. Giriat, J. Appl. Phys. **53**, 7644 (1982).
[28] P. Anderson, Phys. Rev. **79**, 705 (1950).
[29] D. ter Haar and M.E. Lines, Philos. Trans. R. Soc. London, Ser. A **254**, 521 (1962); **255**, 1 (1962).
[30] A. Twardowski, H.J. Swagten, W.J.M. de Jonge, and M. Demianiuk, Phys. Rev. B **36**, 7013 (1987).
[31] V.-C. Lee, Phys. Rev. B **37**, 8849 (1988).
[32] M. Górska and J.R. Anderson, Phys. Rev. B **38**, 9120 (1988).
[33] A. Bruno and J.P. Lascaray, Phys. Rev. B **38**, 9168 (1988).
[34] R.R. Galazka, W.J.M. de Jonge, A.T.A.M. de Waele, and J. Zeegers, Solid State Commun. **68**, 1047 (1988).
[35] Qun Shen, H. Luo, and J.K. Furdyna, Phys. Rev. Lett. **75**, 2590 (1995).
[36] S.-S. Yu and V.-C. Lee, J. Phys.: Condens. Matter **4**, 2961 (1992).
[37] S.-H. Wei and A. Zunger, Phys. Rev. B **48**, 6111 (1993).
[38] T.M. Rusin, Phys. Rev. B **53**, 12 577 (1996).
[39] V. Bindilatti, E. ter Haar, N.F. Oliveira, Jr., Y. Shapira, and M.T. Liu, Phys. Rev. Lett. **80**, 5425 (1998).
[40] V. Bindilatti, E. ter Haar, N.F. Oliveira, Jr., Y. Shapira, and M.T. Liu, J. Appl. Phys. **85**, 5950 (1999).
[41] H. Malarenko, Jr., V. Bindilatti, N.F. Oliveira, Jr., M.T. Liu, Y. Shapira, and L. Puech, Physica B **284-288**, 1523 (2000).
[42] S.-S. Yu and V.-C. Lee, Phys. Rev. B **52**, 4647 (1995).
[43] I. Dzialoshinski, J. Phys. Chem. Solids **4**, 241 (1958).
[44] T. Moriya, Phys. Rev. **120**, 91 (1960).
[45] F. Keffer, Phys. Rev. **126**, 896 (1962).
[46] N. Samarth and J.K. Furdyna, Solid State Commun. **65**, 801 (1988).
[47] B.E. Larson and H. Ehrenreich, Phys. Rev. B **39**, 1747 (1989).
[48] B.E. Larson and H. Ehrenreich, J. Appl. Phys. **67**, 5084 (1990).
[49] L.M. Claessen, A. Wittlin, and P. Wyder, Phys. Rev. B **41**, 451 (1990).
[50] D.L. Huber, J. Appl. Phys. **69**, 6112 (1991).
[51] J.L. Martin, M. Goiran, Z. Golacki, J. Leotin, and S. Askenazy, Phys. Rev. B **50**, 10 680 (1994).
[52] J.P. Lascaray and A. Bruno, J. Phys. Colloq. **C8**, 875 (1988).
[53] A. Bruno and J.P. Lascaray, J. Cryst. Growth **101**, 936 (1990).
[54] K. C. Hass, in *Semimagnetic Semiconductors and Diluted Magnetic Semiconductors*, edited by M. Averous and M. Balkanski (Plenum Press, New York, 1991), p. 59.
[55] T.M. Giebultowicz, J.J. Rhyne, W.Y. Ching, D.L. Huber, and J.K. Furdyna, J. Appl. Phys. **57**, 3415 (1985).
[56] T.M. Giebultowicz, J.J. Rhyne, W.Y. Ching, D.L. Huber, J.K. Furdyna, B. Lebech, and R.R. Galazka, Phys. Rev. B **39**, 6857 (1989).
[57] T.M. Giebultowicz, J.J. Rhyne, J.K. Furdyna, and P. Kłosowski, J. Appl. Phys. **67**, 5096 (1990).
[58] W. Szuszkiewicz, M. Jouanne, E. Dynowska, E. Janik, G. Karczewski, T. Wojtowicz, and J. Kossut, Acta Phys. Pol. A **88**, 941 (1995).
[59] W. Szuszkiewicz, B. Hennion, M. Jouanne, J.F. Morhange, E. Dynowska, E. Janik, and T. Wojtowicz, J. Magn. Magn. Mater. **196/197**, 425 (1999).
[60] W. Szuszkiewicz, B. Hennion, M. Jouanne, J.F. Morhange, E. Dynowska, E. Janik, T. Wojtowicz, M. Zieliński, and J.K.

Furdyna, Acta Phys. Pol. A **94**, 583 (1998).
[61] W. Szuszkiewicz, J.F. Morhange, M. Jouanne, M.A. Kanehisa, R. Świrkowicz, E. Dynowska, E. Janik, T. Wojtowicz, and J. Kossut, Acta Phys. Pol. A **92**, 1025 (1997).
[62] R. Świrkowicz, J. Phys.: Condens. Matter **9**, 6901 (1997).
[63] J. Kossut, Thin Solid Films **267**, 58 (1995).
[64] E. Janik, E. Dynowska, J. Bak-Misiuk, M. Leszczyński, W. Szuszkiewicz, T. Wojtowicz, G. Karczewski, A.K. Zakrzewski, and J. Kossut, Thin Solid Films **267**, 74 (1995).
[65] A.K. Zakrzewski, E. Janik, E. Dynowska, M. Leszczyński, M. Kutrowski, T. Wojtowicz, G. Karczewski, J. Bak-Misiuk, J. Domagała, and J. Kossut, Acta Phys. Pol. A **87**, 433 (1995).
[66] T. M. Giebultowicz and T. M. Holden, in *Diluted Magnetic Semiconductors*, edited by J. K. Furdyna and J. Kossut, Semiconductors and Semimetals, Vol. 25 (Academic Press, Boston, 1988), p. 125.
[67] L. Corliss, N. Elliott, and J. Hastings, Phys. Rev. **104**, 924 (1956).
[68] R.J. Cohen, Phys. Rev. B **48**, 12 813 (1993).
[69] C.L. Henley, J. Appl. Phys. **61**, 3962 (1987); Phys. Rev. Lett. **62**, 2056 (1989).
[70] T.M. Giebułtowicz, J. Magn. Magn. Mater. **54-57**, 1287 (1986).
[71] We will use the terahertz unit to describe the mode frequency. A frequency of 1 THz corresponds to an energy of 4.14 meV, to a wave number of 33.4 cm^{-1}, and to a temperature of 48 K.
[72] U. Steigenberger and L. Lindley, J. Phys. C **21**, 1703 (1988).
[73] T. Holstein and H. Primakoff, Phys. Rev. **58**, 1098 (1940).
[74] N. Bloembergen and T.J. Rowland, Phys. Rev. **97**, 1679 (1955).
[75] M. Bonfante, B. Hennion, F. Moussa, and G. Pepy, Solid State Commun. **10**, 553 (1972).
[76] G. Pepy, J. Phys. Chem. Solids **35**, 433 (1974).
[77] M. Jouanne (private communication).
[78] S. Lovesey, *Theory of Neutron Scattering from Condensed Matter* (Oxford University Press, Fairlawn, NJ, 1984).